

pubs.acs.org/est Article

Ca-Based Layered Double Hydroxides for Environmentally Sustainable Carbon Capture

Sunxiang Zheng, Cuihong Song, Maria C. Curria, Zhiyong Jason Ren, and Claire E. White*



Cite This: Environ. Sci. Technol. 2023, 57, 17212-17224



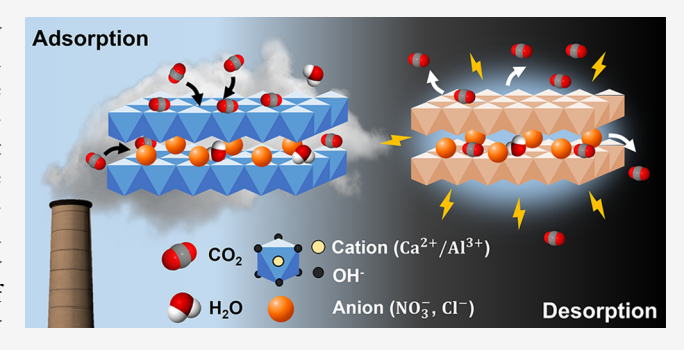
ACCESS I

Metrics & More

Article Recommendations

Supporting Information

ABSTRACT: The process of carbon dioxide capture typically requires a large amount of energy for the separation of carbon dioxide from other gases, which has been a major barrier to the widespread deployment of carbon capture technologies. Innovation of carbon dioxide adsorbents is herein vital for the attainment of a sustainable carbon capture process. In this study, we investigated the electrified synthesis and rejuvenation of calciumbased layered double hydroxides (Ca-based LDHs) as solid adsorbents for CO₂. We discovered that the particle morphology and phase purity of the LDHs, along with the presence of secondary phases, can be controlled by tuning the current density during electrodeposition on a porous carbon substrate. The change



in phase composition during carbonation and calcination was investigated to unveil the effect of different intercalated anions on the surface basicity and thermal stability of Ca-based LDHs. By decoupling the adsorption of water and CO_2 , we showed that the adsorbed water largely promoted CO_2 adsorption, most likely through a sequential dissolution and reaction pathway. A carbon capture capacity of 4.3 ± 0.5 mmol/g was measured at 30 °C and relative humidity of 40% using 10 vol % CO_2 in nitrogen as the feed stream. After CO_2 capture occurred, the thermal regeneration step was carried out by directly passing an electric current through the conductive carbon substrate, known as the Joule-heating effect. CO_2 was found to start desorbing from the Ca-based LDHs at a temperature as low as 220 °C as opposed to the temperature above 700 °C required for calcium carbonate that forms as part of the Ca-looping capture process. Finally, we evaluated the cumulative energy demand and environmental impact of the LDH-based capture process using a life cycle assessment. We identified the most environmentally concerning step in the process and concluded that the postcombustion CO_2 capture using LDH could be advantageous compared with existing technologies.

KEYWORDS: Carbon capture, Ca-based layered double hydroxide, Joule heating, Life cycle assessment

■ INTRODUCTION

The rapid increase of CO₂ concentration in the atmosphere has been causing an unprecedented acceleration of climate change. To achieve the goal of carbon neutrality, 196 countries and regions around the world signed the Paris Agreement in 2015 to address climate change, proposing to achieve net-zero greenhouse gas emissions by the second half of this century.² Among other approaches (e.g., massive adoption of renewable and nuclear energy), carbon capture, utilization, and storage (CCUS) have been proven as viable technologies to reduce greenhouse gas emissions from CO2 heavy industries such as fossil fuel power plants, petroleum refineries, and cement production.^{3,4} For example, it is estimated that over 90% of the CO₂ emissions from the fossil-fuel based power plant can be reduced with CCUS. Although CCUS has been under development for decades, issues around system complexities and high energy costs, especially within the carbon capture stage, have prevented this technology from being extensively implemented. 5,6 For postcombustion capture, emerging solid adsorbents are

believed to be promising alternatives to the prevailing monoethanolamine (MEA)-based CO₂ scrubbing approach due to high capacity, low toxicity, easier handling, and potentially lower energy consumption during the thermal rejuvenation process.⁷ One of the readily developed processes is calcium looping (CaL), during which CO₂ in the flue gas reacts with lime (CaO) to form calcite (CaCO₃). However, the thermal decomposition of the formed CaCO₃ requires an extremely high temperature (typically above 700 °C), ⁸ which is usually achieved using oxy-combustion of fuels. The steam in the calcination atmosphere was reported to catalyze the decomposition reaction but also promotes the deactivation (i.e., sintering) of the adsorbent. ^{9,10} Meanwhile, the urgent

Received: May 17, 2023 Revised: October 5, 2023 Accepted: October 6, 2023 Published: November 2, 2023





need to decarbonize small and distributed carbon dioxide emitters, including small-scale power plants, plastic production, and transportation sectors where the CaL approach is typically not economically feasible, leads to new requirements, such as mild material regeneration conditions and modular system design, for the emerging carbon capture technologies.

Layered double hydroxides (LDHs) are a group of lamellar inorganic solids consisting of bimetallic hydroxide layers intercalated with hydrated anions.11 LDH-derived mixed metal oxides (MMOs), similar to calcium oxide, have been widely studied for medium to high-temperature carbon capture. 12-14 Recently, CO₂ capture from low-temperature gas streams (<100 °C) using pristine LDHs has gained attention due to the large surface area within the interlayer regions and the basic surface chemistry that favors the adsorption of CO₂. 15 In particular, Ca-based LDHs have been found to have higher surface basicity, a property reported to have linear correlation with the carbon capture capacity, 16 than the well-known hydrotalcite (i.e., $[Mg_6Al_2(OH)_{16}]CO_3$ · 4H₂O) because Ca²⁺ is more electronegative with respect to Mg²⁺.¹⁷ Different from other low-temperature CO₂ sorbents such as carbonaceous materials, metal organic frameworks (MOFs), and zeolites, which suffer from reduced adsorption efficiency in a humid gas stream such as a typical flue gas stream (5-15 vol.% of H₂O vapor), ¹⁸ Ca-based LDHs adsorb CO₂ through the formation of chemical bonding in a similar manner to the carbonation of portlandite, during which the adsorption of CO2 is considered to be facilitated by the presence of water vapor. 19 During thermal-based material rejuvenation, the adsorbed surface and intercalated water tend to desorb from the LDHs, causing the collapse of interlayer spaces and the formation of metastable mixed oxides. It has been shown that the layered structure can be recovered by exposure to humid air through the so-called "memory effect". 20 Such unique rehydration and restructuring are essential to the cyclic carbon dioxide adsorption and desorption process. However, the impact of moisture on carbon capture capacity, the formation of secondary phases during structure transformation, and the underlying mechanisms of capture have not been demonstrated. Therefore, to achieve an efficient and resilient carbon capture process utilizing Ca-based LDHs, additional research is required to fundamentally understand the carbonation and calcination cycles.

Besides carbon capture performance, the economic and environmental considerations of emerging carbon capture materials are also important aspects of CCUS, but they are rarely discussed in the literature. Conventional LDH synthesis methods (e.g., coprecipitation and mechanochemical approaches) often involve the dosage and disposal of highly alkaline solutions which have significant environmental impacts.^{21,22} Moreover, the commonly adopted oxyfuel combustion for thermal-based material rejuvenation, as in the case of the CaL process, consumes a considerable amount of fossil fuels, partially offsetting the benefit of CCUS. Therefore, reducing the CO₂ emissions and energy consumption associated with material synthesis and rejuvenation is vital to realizing a sustainable carbon capture process. Detailed "cradleto-grave" analysis is also critical to evaluate the environmental aspects associated with the carbon capture materials and assist with prioritizing improvements in synthesis approaches and system design.

Using electricity as a clean and renewable energy source, here, we adopted an electrodeposition method to directly

deposit Ca-based LDHs on a porous carbon substrate to form a gas filter. The particle morphology and phase purity of the LDH were characterized and controlled by tuning the current density during electrodeposition. Carbon capture capacity and kinetics were measured at various temperatures and humidity conditions to unveil the carbon adsorption mechanism and the role of water vapor. After CO₂ capture occurred on the LDHcarbon filter, we explored material rejuvenation using Jouleheating which was enabled by the electrically conductive carbon substrate. The cyclability of the LDH-carbon filter was also evaluated where the capture capacity as a function of the number of cycles has been quantified. Finally, we analyzed and compared life cycle environmental impacts associated with the proposed process and two widely adopted CCUS approaches (including amine-based scrubbing and CaL processes) for postcombustion carbon capture at a typical fossil fuel power plant. This prospective LCA of scaled-up Ca-based LDHs was performed to offer guidance for practical application, especially during the early phase of research and development with high freedom for advancing LDH-based CCUS approaches.

MATERIALS AND METHODS

Synthesis of the Ca-Based LDH. The Ca-based LDH was deposited in situ on a porous carbon substrate (Freudenberg H23) using an electrodeposition technique. The electrolyte solution consisting of 0.3 M Ca(NO₃)₂ and 0.1 M Al(NO₃)₃ (ACS reagent, 99%, Sigma-Aldrich) was prepared using deionized (DI) water. The carbon substrate was rinsed extensively with ethanol and DI water prior to immersion in the electrolyte solution to remove any potential grease and other contaminants that may have inadvertently been picked up during material transportation and handling. The cleaned carbon substrate with a size of 5 × 5 cm was used directly as the cathode of the electrochemical cell. A platinum wire was used as the inert anode. During electrodeposition, an external voltage was applied across the anode and cathode with a constant current density (i.e., normalized current by the surface area of the cathode). The current density was tuned from 20 to 110 mA/cm², which resulted in the formation of the Ca-based LDH of different morphologies and secondary phases. The synthesized Ca-based LDH was rinsed with DI water to remove the excessive electrolyte solution. We also performed an anion exchange process by soaking the carbon substrate-supported LDH in a 1 M CaCl₂ solution (pH was adjusted to 10 using a dilute Ca(OH)2 solution) for 2 h. As confirmed by Fourier-transform infrared (FTIR) spectroscopy (spectra are shown in the Results and Discussion), the intercalated nitrate ions were replaced with the chloride ions during this process. After anion exchange, the LDH was rinsed again with DI water and dried in the vacuum oven (60 °C, 0.1 bar) for 2 h.

Characterization Techniques. The surface morphology and elemental composition of the Ca-based LDH were characterized using scanning electron microscopy (SEM, FEI Quanta 200) equipped with an energy dispersive X-ray detector (EDX, QUANTA 200) at an accelerating voltage of 20 kV. Attenuated total reflectance-Fourier transform infrared spectra of the LDH samples were obtained at 0.5 cm⁻¹ resolution with N₂ purge (ATR-FTIR, PerkinElmer Frontier FTIR instrument with a universal ATR sampling accessory). A total of 32 scans were accumulated for each spectrum with a scan speed of 1 cm/s. The phase composition of the Ca-based LDH was measured by X-ray diffraction (XRD, Bruker D8

Discover) at 0.05° resolution and a scan speed of 2° /min using Cu K α radiation. X-ray total scattering measurements were performed at ambient temperature, using the 28-ID-1 beamline at the National Synchrotron Light Source II, Brookhaven National Laboratory, using sample-to-detector distance of 220 mm. The monochromatic photon energy was set at 74.465 keV (0.1665 Å). The pair distribution function (PDF, G(r)) was then calculated using the sine Fourier transformation of the measured total scattering function S(Q) as follows

$$G(r) = \frac{2}{\pi} \int_{Q_{min}}^{Q_{max}} Q[S(Q) - 1] \sin(Qr) dQ$$
(1)

where Q is the momentum transfer and defined as

$$Q = \frac{4\pi \sin \theta}{\lambda} \tag{2}$$

where θ and λ are the scattering angle and X-ray wavelength, respectively. PDFs were obtained using PDFgetX2 with a Q_{max} of 20 Å⁻¹ with a smoothing scheme based on averaging data over 20 points starting from a Q value of 8 Å⁻¹ to increase the signal-to-noise ratio. Such smoothing was deemed necessary due to the small amount of sample in the beam (scattering was performed in the transmission geometry through the gas filter). Scattering from the carbon substrate was subtracted from the data using PDFgetX2 prior to the Fourier transformation. ²⁴

To identify the species and amount of gas released from the LDH upon calcination, thermogravimetric analysis (TGA, Pyris 1, PerkinElmer) coupled with transmission-FTIR spectroscopy (PerkinElmer Frontier FTIR instrument) experiments was carried out with a temperature ramping rate of 10 °C/min in N₂. The released gaseous species from the LDH were transferred to the IR cell using a TL 8000 transfer line at a flow rate of 20 mL/min. The temperatures of the transfer line and the IR cell were set at 300 °C and 250 °C, respectively. A single scan from 550 to 4000 \mbox{cm}^{-1} was collected every 60 s with a scan speed of 1 cm/s and a resolution of 4 cm⁻¹. Coupled differential scanning calorimetry and thermogravimetric analysis (Setaram Instrumentation TG-DSC III) was employed to analyze the enthalpy change during calcination from 30 °C to 800 °C with a temperature ramping rate of 10 °C/min in N₂. The N₂ adsorption-desorption isotherms of the LDHs were acquired using a Micromeritics 3Flex instrument after degassing at 60 °C for 2 h. The surface area was calculated following the Brunauer-Emmett-Teller (BET) theory.

Carbon Dioxide Capture Capacity Measurements. The carbon dioxide capture capacity of the LDH loaded carbon filter (LDH-carbon filter) was measured as the total mass change when exposed to CO2 using thermogravimetric analysis (TGA, Pyris 1, PerkinElmer) held at a constant temperature. A schematic diagram of the manifold system design is shown in Figure S1. To decouple the adsorption of water vapor and CO2, we used dry N2 as the purging gas during the initial stage of the test. After the mass of the LDHcarbon filter stabilized, the purging gas was switched to humid N₂, which was achieved by flowing dry N₂ through a gas bubbler containing deionized (DI) water. The relative humidity (RH) of the gas stream was measured at the inlet of the TGA instrument using an RH probe (Fisherbrand Traceable Humidity Meter). When the mass of the LDHcarbon filter had stabilized in the humid N2 gas stream, the purging gas was switched to a humid mixture of 10 vol.% CO2

and 90 vol.% N_2 , which represents the typical CO_2 level in flue gas from coal-fired power plants. Once again, the humidity was provided by flowing the CO_2/N_2 mixed gas stream through a bubbler containing DI water. The temperature was held constant at 30 °C, 60 °C, 90 °C, and 150 °C during the tests. For each test ~10 mg of the sample (LDH-carbon filter) was placed in the platinum crucible on the TGA instrument.

pubs.acs.org/est

Material Rejuvenation and Long-Term Stability Tests. The thermal rejuvenation of the LDH-carbon filter was performed by passing an electric current through the conductive carbon substrate. The released H₂O and CO₂ were carried by a N₂ purge gas and analyzed using a H₂O/ CO2 detector (LI-840 A, LI-COR) with a data collection interval of 1 s. To evaluate the long-term stability, LDH-carbon filters were first exposed to CO2 in a carbonation chamber (Thermo Scientific Forma Steri-Cult CO2 incubator) with 10 vol.% CO2, 50% RH at 30 °C for 2 h to reach the full CO2 capture capacity. The LDH-carbon filters were then rejuvenated by using Joule-heating. Briefly, LDH-carbon filters with a size of 5 cm \times 5 cm were connected to a power supply (3644A, Circuit Specialists Inc.) using two copper clamps. To evenly distribute the current, two strips of stainless steel mesh $(0.5 \text{ cm} \times 5 \text{ cm})$ were placed on each side of the LDH-carbon filter as current collectors. The copper clamps ensured close contact between the current collector and the LDH-carbon filters. The surface temperature of the LDH-carbon filters was monitored by using a thermal camera (FLIR TG297). The current that passed through the LDH-carbon filters was adjusted until the surface temperature reached a maximum of 600 °C. The total power output was read from the power supply. The cumulative amounts of released H₂O and CO₂ over a period of 5 min were integrated. After rejuvenation, we returned the LDH-carbon filter to the carbonation chamber and repeated this process 10 times (i.e., 10 cycles, each cycle consisting of capture and rejuvenation).

Life Cycle Assessment and Techno-Economic Analysis of Carbon Capture Technologies. The LDH-based process achieves CO₂ capture through carbonation (at 30 °C) and Joule-heating-based desorption (maximized at 600 °C) cycles. Detailed experimental parameters and performance of the laboratory-scale LDH are described in Table S1. The laboratory-scale LDH was scaled up according to energy and mass balances, empirical calculations, and similar technical information. The scaled-up LDH was assessed for post-combustion carbon capture in a 500 MWe pulverized coal power plant as described in Petrescu et al. ²⁵ A schematic diagram for a pulverized coal power plant with conceptual LDH postcombustion CCUS is illustrated in Figure S2.

Goal and Scope Definition. A prospective LCA of the scaled-up LDH process was performed to identify the key contributors to environmental impacts and explore the competitiveness of the LDH process compared with two typical postcombustion CCUS technologies, including methyldiethanolamine (MDEA) and calcium looping (CaL). The system boundary included all processes associated with energy generation and carbon capture and storage, that is (1) power production from coal coupled to energy efficient CCUS technologies, (2) upstream processes such as extraction, processing, and transportation of coal, limestone, and solvents used in the power plant and for carbon capture and storage, and (3) downstream processes in terms CO₂ compression, transport, and storage (Figure S2). The construction of infrastructure (e.g., power plants, a CO₂ transportation

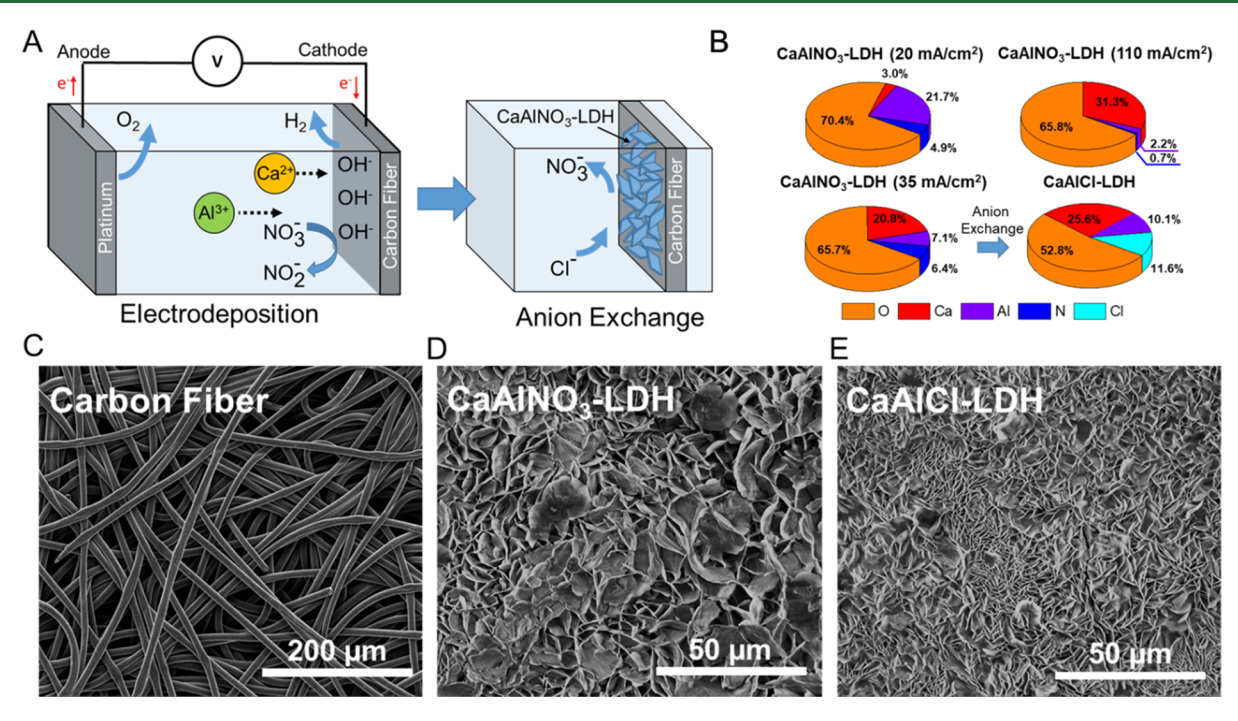


Figure 1. Synthesis of Ca-based LDHs. Schematic illustration of the synthesis route that consisted of electrodeposition and anion exchange (A). The atomic percentage of elements in the synthesized LDH samples was determined by EDX (B); the values in parentheses are the current density used during electrodeposition. SEM images showing the surface morphology of the carbon fiber substrate (C), the CaAlNO₃-LDH synthesized using 35 mA/cm² (D), and the CaAlCl-LDH after anion exchange (E).

pipeline, and CCUS-related tanks) and electricity transmission and distribution were excluded from the analysis. The functional unit was defined as one MWh of net electric power produced in the plant for comparison.

Life Cycle Inventory Analysis. Life cycle inventory (LCI) of the coal power plant applying a scaled-up LDH process was compiled by including all inputs and outputs for producing one MWh of net electric power. To make a systematic comparison between the scaled-up LDH process and two other postcombustion strategies (MDEA and CaL) studied by Petrescu et al., we adopted the same main design assumptions of the coal power plant (i.e., coal moisture, boiler heat losses, and limestone slurry, refer to Table 1 in Petrescu et al. 25). The technical key performance indicators of the plant using various postcombustion CCUS technologies are reported in Table S1. The LCI of the scaled-up LDH process was calculated based on coal flow rate, CO₂ flux in flue gas, and the laboratory-scale LDH data. The LCI for the laboratory-scale LDH process was compiled based on the experimental data acquired in this study. Material, chemical, and energy usage for producing 1 kg of fresh LDH-carbon filters (Table S2) was calculated according to preparation and drying processes as described in material synthesis. The LDH capture capacity (4.28 mmol/ g) was the average value based on a long-term experiment conducted in this study. Electricity consumption during Jouleheating rejuvenation was calculated by using power output, current density, and reaction time. Due to capacity loss of LDH-carbon filters over time, we considered degradation of the LDH and carbon fiber substrate, which were assumed to be 1.1% for each carbonation and rejuvenation cycle based on the experimentally measured capacity loss over 10 cycles. A detailed inventory and the main assumptions of the LDH system are provided in Note 2 of the SI.

Life Cycle Impact Assessment. The environmental impacts of each individual element were calculated using the ReCiPe 2016 Midpoint (H) V1.04 method, based on inputs from the Ecoinvent 3 database embedded in SmaPro 9.1. We investigated 11 typical impact categories measured by the potential of ecosystem-related categories such as global warming potential (GWP), stratospheric ozone depletion, terrestrial acidification, freshwater eutrophication, health-related categories of ozone formation, human carcinogenic toxicity, human noncarcinogenic toxicity, and resource-related categories of land use and water consumption.

Techno-Economic Analysis. Two economic metrics, the levelized cost of electricity (LCOE) and the CO_2 avoidance cost ($\mathrm{C}_{\mathrm{CO2}}$), were calculated to compare economic performances of various CCUS technologies. LCOE is composed of the total capital cost and operation and maintenance costs. $\mathrm{C}_{\mathrm{CO2}}$ is widely used to measure extra investments for avoiding CO_2 emissions from fossil fuel power plants by implementing CCUS technologies. Detailed calculations of LCOE and $\mathrm{C}_{\mathrm{CO2}}$ are provided in Note 2 of the SI.

RESULTS AND DISCUSSION

Controlled Electrodeposition of Ca-Based LDHs. Using Al³⁺ as the trivalent cation, Ca-based LDHs have a brucite-like sheet structure with an ordered arrangement of Ca²⁺ and Al³⁺ ions in seven- and six-coordination, respectively.²⁶ Due to the difference in ionic size, the ratio between Ca²⁺ and Al³⁺ is found to be fixed at the ratio of 2:1,²⁷ rather than having a large range of variation as in the case of hydrotalcite-like materials (with a Mg/Al ratio typically in the range of 1 to 6 and as high as 23.8).²⁸ Therefore, secondary phases are more likely to form in the Ca-based system using the widely adopted coprecipitation method as all the reactants are mixed at the same time.²⁹ To better control the reaction

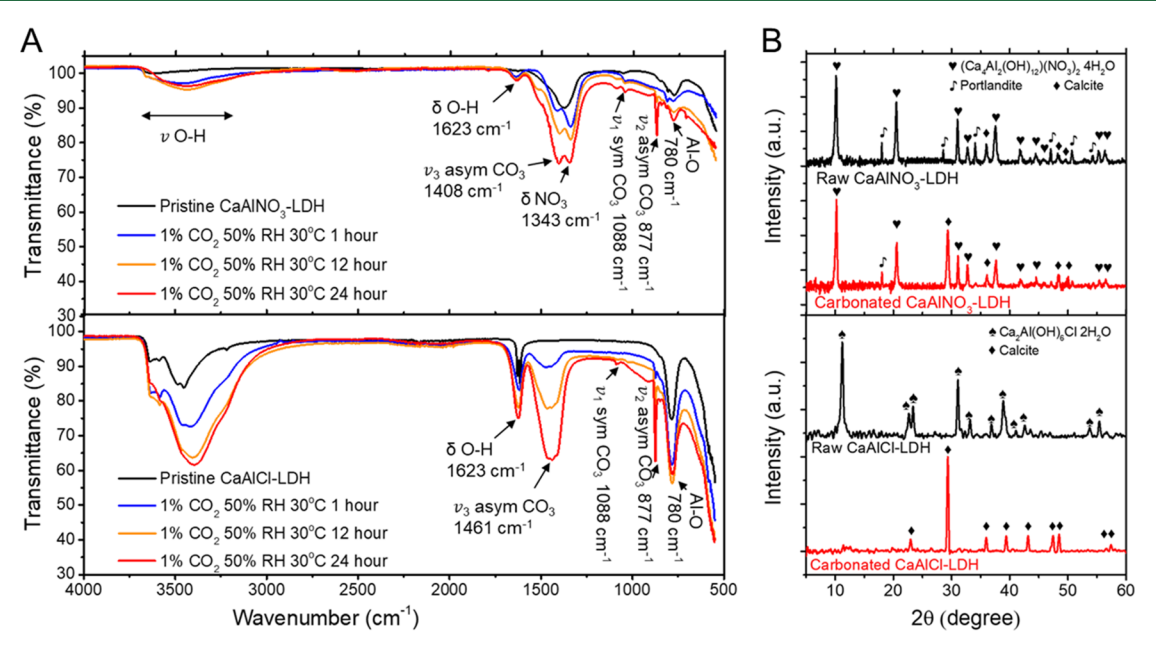


Figure 2. Structural analysis of Ca-based LDHs during carbonation. FTIR spectra of the CaAlNO₃-LDH and the CaAlCl-LDH show a notable intensity increase of both the $-CO_3$ and water peaks as a result of carbonation (A). X-ray diffraction patterns of CaAlNO₃-LDH (top) and CaAlCl-LDH (bottom) before and after carbonation for 24 h (B).

between each component, electrodeposition of the Ca-based LDH was performed using different current densities. As shown in Figures 1A and 1C, we used a porous substrate made from nonwoven carbon fibers as the cathode of the electrochemical cell. Nitrate was selected as the anion in the electrolyte because nitrite reduction starts at a more positive potential than hydrogen evolution and therefore reduces the formation of $\rm H_2$ bubbles on the carbon fiber surface. Two cathodic reactions occur concurrently at the surface of the carbon substrate under the applied external voltage range of -1.5 to -2.0 V vs SHE. No ammonia was detected after the electrodeposition (detection limit ~ 0.01 mg/L).

$$NO_3^- + H_2O + 2e \rightarrow NO_2^- + 2OH^ E^0_{25^{\circ}C} = 0.01 \text{ V vs. SHE}$$
 $2H_2O + 2e \rightarrow H_2(g) + 2OH^ E^0_{25^{\circ}C} = -0.828 \text{ V vs. SHE}$

The cations are electrically driven toward the cathode surface where they meet the hydroxide ions and form Ca-based LDHs. Since a mole of OH⁻ can be produced by passing one mole of electron through either reaction pathway above, the local pH at the carbon substrate surface will be strongly correlated with the applied current density.³⁰ Therefore, a constant current density was supplied to maintain a steady generation of OH and thus a high pH in the vicinity of the precipitating Ca-based LDH. At a low current density (i.e., 20 mA/cm²), a thin layer of solid is found to precipitate on the cathode forming a flat layer parallel to the cathode surface (Figure S3). Elemental analysis of the precipitated solid suggests a low Ca:Al molar ratio of 1:7 (Figure 1B), which is significantly different from the typical ratio found in hydrocalumite-like materials (i.e., 2:1).³¹ Further analysis via XRD of the solid indicates the presence of Al(OH)₃ (Figure S3). Conversely, a high current density (i.e., 110 mA/cm²) leads to a thick layer of precipitate with a high Ca to Al molar ratio of 15:1 (Figure 1B), due to the formation of portlandite (Figure S3). At the intermediate current density range (i.e., 35 mA/ cm²), the Ca-based LDH with a chemical composition of [Ca₂Al(OH)₆]NO₃·2H₂O (denoted as CaAlNO₃-LDH) forms

as the dominant phase. A small amount of portlandite also forms as the secondary phase as indicated by the Ca to Al molar ratio in the precipitate (~3:1 instead of 2:1) and the existence of characteristic peaks of portlandite in the XRD pattern (Figure 1B and Figure S3, respectively).

To understand the impact of applied current density on secondary phase formation, the concentration of aqueous species and the saturation indices of solid phases as a function of pH were calculated based on the initial electrolyte concentration and the solubility product constants (K_{sn}) of the secondary phases. As the local pH increases from the bulk pH value (i.e., pH of 3, measured using pH meter), the solubility of aluminum species decreases and reaches a minimum at a pH of 6.5 (Figure S4). Indeed, insoluble Al(OH)₃ is seen to precipitate in our synthesis process by using a low current density. Based on the reported log K_{sp} values for other Me(II)-Al LDHs (i.e., $-17.9 \sim -25.7$), $\stackrel{32}{\sim}$ the saturation indices of Ca-based LDHs are estimated to reach zero for a pH range between 4.7 and 7.3, at which point the deposition of CaAlNO₃-LDH commences. At a higher current density, the local pH is believed to increase beyond a pH of 12, and hence the formation of portlandite becomes dominant, whereas the solubility of Al(OH)₃ increases with the pH and the saturation indices of Al(OH)₃ also drop below zero when the pH is greater than 13.6 (Figure S4). Moreover, the rate of OH generation, as controlled by the current density, also affects the growth direction of the LDH. It was previously pointed out that a steep concentration gradient of electrolytes near the cathode surfaces could lead to the horizontal growth of LDHs, whereas a smoother concentration gradient often results in the growth of vertically aligned LDHs.³³ Such phenomena have also been observed in this study by varying the concentration gradient of OH-. Vertically aligned LDHs have been synthesized by fine control of the current densities between 35 and 95 mA/cm² (Figure S3 and Figure 1D). The vertically grown LDHs are preferred for CO2 adsorption because of the higher surface area and more exposed interlayer regions. Therefore, a current density of 35 mA/cm² has been

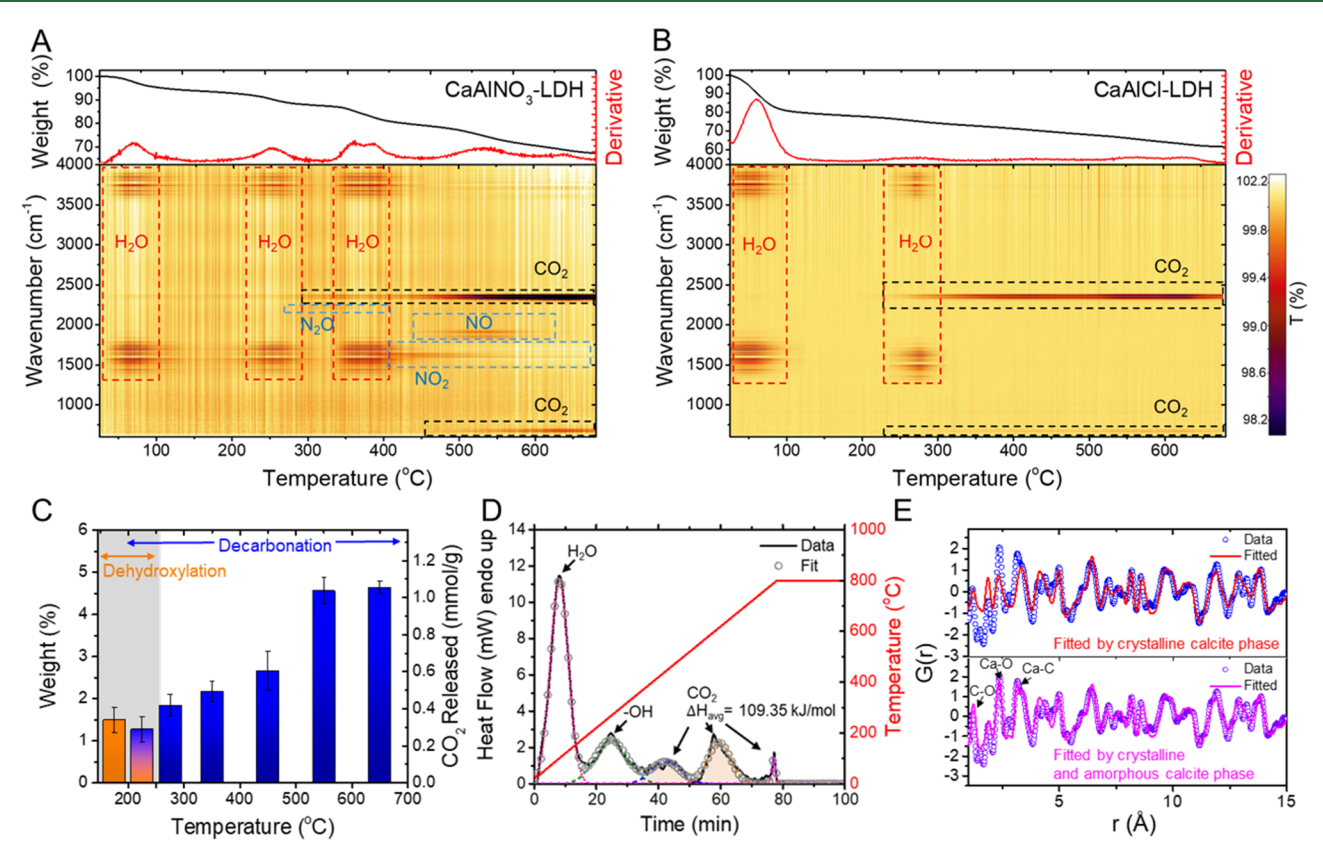


Figure 3. Rejuvenation of Ca-based LDHs using thermal treatment. Thermogravimetric and differential thermal analysis curves of carbonated CaAlNO₃-LDH (A) and CaAlCl-LDH (B). Both LDH samples were carbonated in 1 vol % CO₂ and 50% RH at 30 °C for 24 h. The time-resolved FTIR spectrum (bottom) was coupled with thermogravimetric analysis to identify the gas species released from the LDH at different temperatures. The results of the stepwise isothermal scan quantify the amount of the CO₂ desorbed for specific temperature ranges (C). Differential scanning calorimetry analysis of carbonated CaAlCl-LDH reveals the enthalpy change during decarbonation (D). Pair distribution function analysis showing carbonated CaAlCl-LDH modeled using calcite and amorphous gibbsite (top) and calcite, amorphous gibbsite, and amorphous calcium carbonate (bottom) (E).

selected for the subsequent investigation of the $\rm CO_2$ capture performance. Mass loading of 1 g LDH/g carbon substrate has been achieved after 5 min of electrodeposition. The BET surface area of the synthesized CaAlNO₃-LDH as probed using N₂ adsorption is found to be 26 m²/g (Figure S5). Note that such surface area does not include contributions from the interlayer regions (these regions collapsed during the necessary pretreatment for N₂ sorption analysis), which may also be active sites for carbon capture.

A unique feature of LDHs in general is the versatility in the type of intercalated anion. The charge density of the anions is believed to be correlated with the surface basicity of the LDHs, which is a critical parameter for CO₂ adsorption capacity and selectivity.³⁴ Here, a liquid phase anion exchange has been performed to switch the intercalated anion to Cl-, which has a higher charge density than the original NO₃⁻³⁵ The surface morphology of the Ca-based LDH remains largely unchanged after anion exchange (Figure 1E). Elemental analysis of the final product with a chemical composition of Ca₂Al(OH)₆Cl· 2H₂O (denoted as CaAlCl-LDH) reveals a reduced Ca:Al molar ratio of 2:1 (Figure 1B). The loss of calcium is likely due to the partial dissolution of portlandite in the anion exchange solution (pH = 10). Indeed, the XRD pattern shows a high purity CaAlCl-LDH phase without noticeable characteristic peaks of portlandite that were found in the original CaAlNO₃-LDH (Figure 2B). The BET surface area of CaAlCl-LDH also

increases to $37 \text{ m}^2/\text{g}$, likely due to the absence of low-surface-area secondary phases (Figure S5).

Structural Changes during Carbonation and Calcination. To understand the CO₂ adsorption and desorption mechanisms, the molecular structural changes of Ca-based LDHs during carbonation and calcination were characterized (Figure 2 and Figure 3). The FTIR spectrum of the asprepared CaAlNO₃-LDH shows a characteristic peak of NO₃ at 1343 cm⁻¹ and weak -OH peaks at 1623 cm⁻¹ and around 3400 cm⁻¹ (Figure 2A). The XRD pattern of the as-prepared CaAlNO₃-LDH suggests the presence of portlandite as a secondary phase.³⁶ During the 24 h carbonation period, the intensity of the FTIR carbonate peak only increases by a factor of 0.25 with respect to the -NO₃ peak, which is assumed to remain constant during carbonation. Analysis of the XRD pattern shows the emergence of calcite peaks after carbonation (Figure 2B). However, the LDH phase is still the dominant phase even after carbonation. The reduced signal of portlandite indicates that this secondary phase also contributes to CO2 adsorption.

During the anion exchange process, the secondary phase formed in the electrodeposited LDH mostly dissolves, leaving phase-pure CaAlCl-LDH, as depicted by the XRD pattern (Figure 2B). The dissolution of portlandite can be explained by the reduced basicity of the anion exchange solution (i.e., pH = 10), which leads to negative saturation indices of portlandite (Figure S4). The absence of the NO_3 peak in the FTIR

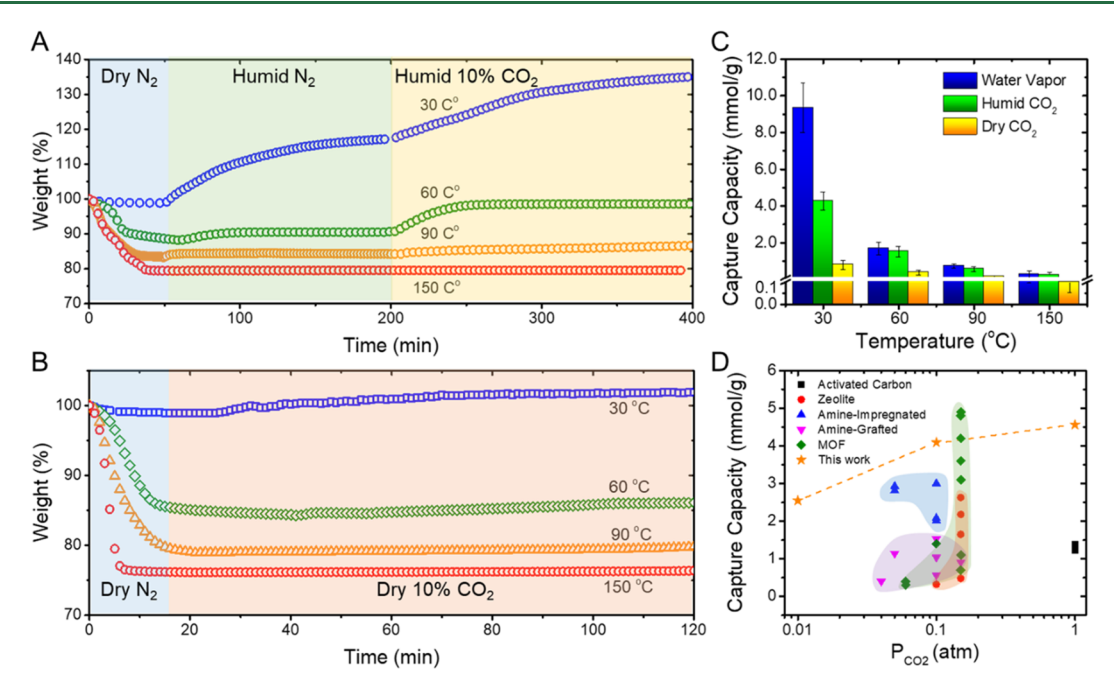


Figure 4. Carbon capture capacity of Ca-based LDHs. Isothermal gravimetric analysis of CO_2 adsorption by CaAlCl-LDH at different temperatures in the presence of water vapor (\sim 1.2 mmol H_2O per mol mixed gas) (A) and in the dry condition (B). Temperature was held constant in the TGA instrument for each test. Summary of the temperature and RH effect on CO_2 adsorption capacity (C). Comparison of carbon capture capacity of different solid adsorbents at temperatures between 25 to 30 °C (D).

spectrum of CaAlCl-LDH also suggests the complete replacement of NO₃ anions. Another notable feature of CaAlCl-LDH shown in the FTIR spectrum is the more pronounced OH peaks at 1623 cm⁻¹ and around 3400 cm⁻¹, indicating an enhanced hydration level. Over the course of 24 h carbonation, the intensities of the carbonate peaks and OH peaks in the FTIR spectrum of CaAlCl-LDH increase significantly, suggesting the adsorption of both water and CO₂. Meanwhile, the XRD pattern of the carbonated CaAlCl-LDH consists solely of calcite, indicating a high level of carbonation. Although the XRD pattern indicates the formation of highly crystalline calcite, a slight shift of the carbonate peak toward higher wavenumber (1461 cm⁻¹) in the FTIR spectrum also suggests the potential presence of amorphous carbonate phases.³⁷

The weight loss during thermal decomposition and the gas species generated from the Ca-based LDHs were monitored using TGA coupled with an in situ transmission-FTIR. The carbon substrate was determined to be thermally stable below 800 °C and thus does not pose interference with the TGA and FTIR data (Figure S6). Both CaAlNO₃-LDH and CaAlCl-LDH lose adsorbed water at a temperature below 150 °C (Figures 3A and 3B). The weight loss in this temperature range is more significant (~20 wt %) for the CaAlCl-LDH, which again confirms its higher hydration level (Figure 3B). The second water loss event happens at temperatures between 200 °C and 300 °C for both Ca-based LDHs, mainly due to the dehydroxylation from the LDH basal plane.³⁸ Notably, CaAlNO3-LDH has a greater weight loss than CaAlCl-LDH due to the lower carbonation level (i.e., more exposed hydroxide) and the presence of secondary hydroxylated phases that remain after the carbonation process. Over a similar temperature range, the decomposition of the interlayer carbonates commences and continues with rising temperature. However, due to their low charge density, the NO₃ ions are

found to be less thermally stable compared with Cl ions. The several weight loss events of CaAlNO $_3$ -LDH associated with the release of water and NO $_x$ at 350 $^{\circ}$ C and above can be attributed to the decomposition of NO $_3$. Such poor thermal stability severely limits the application of CaAlNO $_3$ -LDH as a viable adsorbent for carbon capture. Therefore, CaAlCl-LDH was selected for further characterization and tests.

To quantify the desorption of CO₂ at different temperature ranges, stepwise isothermal scans were performed. TGA-FTIR analysis shows that the decarbonation of CaAlCl-LDH commences at a temperature around 200 °C and peaks at around 600 °C (Figures 3B and 3C). Because of the overlapping weight loss events of dehydroxylation and decarbonation at a temperature between 200 and 250 °C, we temporarily exclude the CO2 released below 250 °C for quantification of CO2 adsorption capacity. Around 40% of the total adsorbed CO2 is released below 500 °C, above which a complete desorption of CO₂ can be achieved at around 700 °C (Figure 3C). The modest initiation temperature required for CO₂ desorption presents an opportunity for processes that rely on less energy-intensive thermal sources. DSC-TGA analysis of the carbonated CaAlCl-LDH shows three decarbonation peaks between 300 and 800 °C, indicating the coexistence of multiple carbonate phases (Figure 3D). The first broad peak centered at around 400 °C is likely due to the desorption of the intercalated carbonate between the LDH layers. 40 The second decarbonation peak found at around 600 °C is likely due to the decomposition of the carbonate phase that directly bonds to the LDH surfaces. The third decarbonation peak observed at 780 °C closely resembles the thermal decomposition peak of calcite (Figure S7), indicating the presence of crystalline carbonate phases similar to calcite. The averaged enthalpy change for the decarbonation of CaAlCl-LDH is 109.4 kJ/mol CO2, more than 30% less than the energy required for calcite decomposition (168.8 kJ/mol CO₂ based

on DSC-TGA analysis, Figure S7).⁴¹ To better understand the link between the CO₂ desorption temperature and the structure of the carbonated CaAlCl-LDH, synchrotron-based high energy X-ray diffraction and subsequent pair distribution function (PDF) analysis were performed, where we used a crystalline calcite phase and an amorphous gibbsite phase as the initial structures for phase refinement. Notably, there is some major disagreement between the model fit and the experimental data at short distances (r < 5 Å), as seen in Figure 3E. The intensities of the Ca-O correlation (2.36 Å) and Ca-C correlation (3.17 Å) of the model fit are significantly lower than the experimental data. Contrarily, the fit quality is reasonably good at higher interatomic distances. Such phenomena often relate to the absence of an amorphous phase in the model fitting since the structural signals of amorphous phases diminish with increasing r-range. Indeed, the model fitting is improved by adding an amorphous calcite phase (with the nanocrystalline size set to 5 Å), which indicates the presence of an amorphous carbonate phase in the carbonated CaAlCl-LDH. The amorphous phase is a metastable state, of which the free energy is larger than that of the crystalline state, and therefore requires less activation energy for thermal decomposition.

The composition change of carbonated CaAlCl-LDH and the formation of new secondary phases during calcination were further characterized using XRD. At a calcination temperature below 200 °C, the XRD pattern of carbonated CaAlCl-LDH remains solely of calcite (Figure S8). The formation of calcium aluminum oxides is seen to occur when calcinated at 400 °C. At an even higher calcination temperature, the partial change of Ca and Al local bonding environments and amorphization occurs, generating a portion of single-component crystalline metal oxides including CaO and Al₂O₃ (Figure S8) 42 along with the likely presence of an amorphous mixed metal oxide.⁴ However, the metastable metal oxides and intercalated Cl ions can go through a hydration process and partially recover the LDH structure by absorbing water vapor. After resting in a humid environment (~65% RH) for 2 h, the 003 peak is seen to reappear in calcinated LDHs, indicating the recovery of a layered structure with absorbed water in the interlayer galleries. However, the reduced intensity of crystalline phases and prevalence of an amorphous content suggests some decomposition or irreversible transformation of the LDH has occurred.44

Carbon Capture Performance and the Role of Water **Vapor.** To decouple the adsorption of CO₂ and water vapor on CaAlCl-LDH surfaces and unveil the role of water vapor in the carbon capture process, the adsorption of water vapor and CO₂ was measured sequentially. The adsorption of water vapor was tested by purging humid N₂ (RH of 40%) into the TGA where the sample was held at a constant temperature (Figure 4A). At 30 °C, the adsorption of water vapor reaches a plateau of ~20 wt % after 150 min. At 60 °C, the water adsorption capacity of the CaAlCl-LDH decreases significantly to ~2 wt %, which further decreases to less than 1 wt % at an even higher temperature (over 90 °C). To unveil the adsorption mechanism, the experimental data were fitted using both firstorder and second-order kinetic models, and the rate constants were then used to obtain the thermodynamic parameters. It is found that the adsorption kinetics of water vapor can be well represented ($R^2 = 0.9997$) by a pseudo-first-order kinetic model with a reaction rate constant of 0.018 min⁻¹ at 30 °C (Figure S9). At 60 and 90 °C, the adsorption rate constant of water increases by a factor of 3.7 and 7.9, respectively, likely due to the enhanced diffusion at the higher temperature. ⁴⁵ The apparent activation energy is found to be 38.8 kJ/mol using the Arrhenius equation (Figure S10), indicating that the dominating adsorption mechanism is likely to be physisorption and the rate-limiting step could be surface diffusion. ⁴⁶

The impacts of water vapor on carbon capture were examined by feeding 10% CO2 and 90% N2 under humid (~1.2 mmol H₂O per mol mixed gas, Figure 4A) and dry (Figure 4B) conditions. The results show that the existence of water vapor increases adsorption of CO2 by up to six times compared with dry conditions (Figure 4C), indicating the importance of water vapor in the carbon capture process. This is consistent with previous findings that moisture in the air can greatly accelerate the carbonation of Ca(OH)2 by the increased concentration of protons in the presence of CO_2 (i.e., $H_2O + CO_2 \rightarrow 2H^+ + CO_3^{2-}$).⁴⁷ In addition to water vapor, temperature also plays a vital role in the adsorption of CO₂ since the carbon dioxide absorption capacity is seen to gradually diminish as the temperature increases. The equilibrium adsorption capacity is found to be 4.28 \pm 0.49 mmol/g at 30 °C, which decreases to 1.52 \pm 0.28 mmol/g at 60 °C and less than 0.5 mmol/g at temperatures over 90 °C (Figure 4C). The adsorption kinetics of CO₂ was fitted using the pseudo-second-order kinetic model ($R^2 = 0.9913$) with the apparent activation energy being 56.9 kJ/mol, indicating the adsorption of CO₂ involves chemical reactions.⁴⁸ Comparing the molar mass of adsorbed water vapor and CO₂, the amount of water vapor is found to be much higher than CO₂ at 30 °C (Figure S11). At a higher temperature, the molar mass of adsorbed CO₂ approaches roughly the same as the molar mass of adsorbed water molecules, implying that the CO₂ adsorption could be limited by the amount of adsorbed water.

Figure 4D summarizes and compares the carbon capture capacity of CaAlCl-LDH with those of other solid sorbents under the same testing conditions. Physisorbents such as MOFs and zeolites show a carbon capture capacity up to 5 mmol/g at a CO₂ partial pressure of 0.1 atm and above. However, because of the weak bonding force involved in the physisorption process, the adsorption capacity significantly drops with a decrease in the CO₂ partial pressure. The presence of water vapor might further reduce the carbon capture performance due to competitive adsorption on active sites. Amine-grafted porous sorbents typically can adsorb CO2 both physically and chemically.⁵² The adsorption is more selective due to the formation of covalent bonds and hence is less affected by the reduced partial pressure of CO2. As a comparison, the CO₂ adsorption capacity of CaAlCl-LDH outperforms the amine-based chemisorbents and is comparable with the nanoporous physisorbent such as MOF in 10% CO₂. Notably, CaAlCl-LDH exhibits a moderate decline of capture capacity with reduced CO₂ partial pressure (i.e., 2.5 mmol/g in 1% CO₂), making it a promising candidate for direct air capture. However, the decarbonation of CaAlCl-LDH would require a higher temperature compared with the listed adsorbents due to the formation of strong chemical bonding. Therefore, we found CaAlCl-LDH a more suitable sorbent for postcombustion carbon capture where thermal energy is readily available. Further investigation is required to evaluate the economic feasibility of this material as a solid sorbent for direct air capture.

Electrothermal Material Rejuvenation and Cyclability. Using electricity as a clean and renewable energy source,

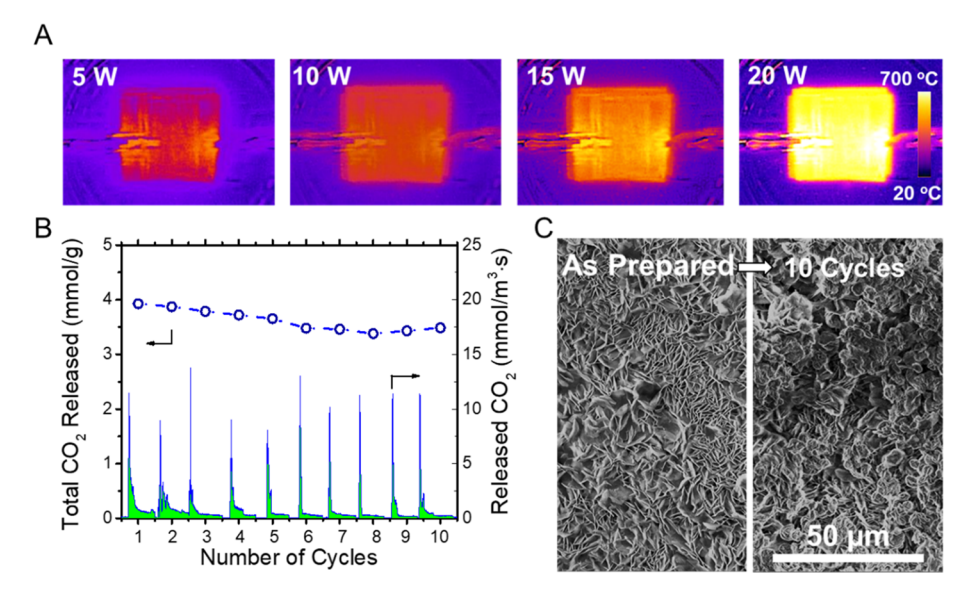


Figure 5. Joule-heating-based material rejuvenation. Surface temperature monitoring was done using a thermal camera as a function of applied current density (A). The CO_2 desorption rate and the total amount of CO_2 desorbed in ten consecutive cycles, with a 5 min duration for each desorption cycle (B). SEM image showing the surface morphology change at the end of the tenth cycle (C).

we explored the rejuvenation of carbonated CaAlCl-LDH using Joule-heating. Compared with the conventional calcination process, which involves combustion of fossil fuels in highly pure oxygen, the Joule-heating process may offer better precision and higher controllability and hence be more adaptable for small-scale operations. To maximize heat production, the LDH-carbon filters were stacked into a multilayer configuration (i.e., functionally similar to a parallel circuit). Such a configuration has the potential to produce more heat and reduce convective energy losses to the carrying gas since only the top and bottom surfaces of the filters are exposed directly to the gas stream. As shown in Figure S12, the electrical power required for heating each of the LDH-carbon filters to a rejuvenation temperature of 700 °C decreases as more filters are stacked. We found that the LDH-carbon filters are homogeneously heated with the surface temperature increasing linearly with the applied power density (Figure 5A and Figure S12). Since the Joule-heating effect occurs directly on the porous carbon substrate where the LDHs are attached, heat transfer is believed to be highly efficient.⁵⁵

To evaluate the carbon capture cyclability of CaAlCl-LDH, 10 cycles of carbonation and Joule-heating-based calcination were conducted. During the decarbonation (i.e., calcination) process, the amount of released CO₂ is seen to spike within the first 30 s and then decreases rapidly (Figure 5B). When running at a lower power density (i.e., lower surface temperature), the release of CO₂ spikes in a similar time frame, while the total amount of CO2 decreases with the temperature, indicating that thermal decomposition is mainly thermodynamic-limited rather than kinetics-limited (Figure \$13). Due to the fast temperature ramping using the Jouleheating process, over 95 wt % of adsorbed CO2 can be released in 5 min, largely saving the rejuvenation time and energy. Due to the porous microstructure of the deposited CaAlCl-LDH and low thermal expansion coefficient of the fibrous carbon substrate, no delamination of the sorbents was observed after 10 cycles. However, some performance decline was observed throughout the sorption/desorption cycles. Around 11.4% of the capacity is lost at the end of the 10th cycle, and surface

sintering of the layers occurs (Figure 5C) which is partially responsible for the capacity loss. We also found that most of the sintering happens at the outer surface, whereas the LDH particles originally attached to the carbon fibers retain their layered structure. Similar enhancement of stability has also been reported for LDHs supported by carbonaceous materials such as graphene and carbon nanotubes. 54,55 As a comparison, CaO, the sorbent used in CaL process, can lose more than half of the sorption capacity in 10 cycles due to sintering-induced decay of surface porosity.⁵⁶ Although Joule heating offers several advantages, such as precise temperature control and reduced material sintering, combining it with a well-designed looping system such as that used for CaL would further enhance its benefits. An automated looping system with electric resistance heating would allow for seamless sorbent replacement, precise temperature regulation, and efficient heat transfer, making it an even better option for calcination processes, especially in terms of sustainability and costeffectiveness.

Life Cycle Assessment and Techno-Economic Analysis for Postcombustion Capture Using Ca-Based LDHs.

Despite the recent emergence of many novel solid sorbents for carbon capture, few LCA studies exist that evaluate the environmental impacts of these materials, such as global warming potential (GWP), acidification potential (AP), and water consumption (WC). Emerging solid adsorbents, including Ca-based LDHs, MOFs, and amine-grafted porous sorbents, typically involve multiple chemical precursors and sophisticated synthesis steps, which potentially produce more carbon emissions compared with the readily available solvents/ sorbents that have been used thus far in industry. Therefore, a preliminary LCA has been conducted to compare the environmental performance of LDH carbon filters with other similar technologies (i.e., MDEA and CaL) and identify potential pathways for further optimization. All carbon capture technologies considered in this investigation are postcombustion and assumed to run in carbonation and rejuvenation cycles for postcombustion carbon capture in a 500 MWe pulverized coal power plant with capacity loss identified in the

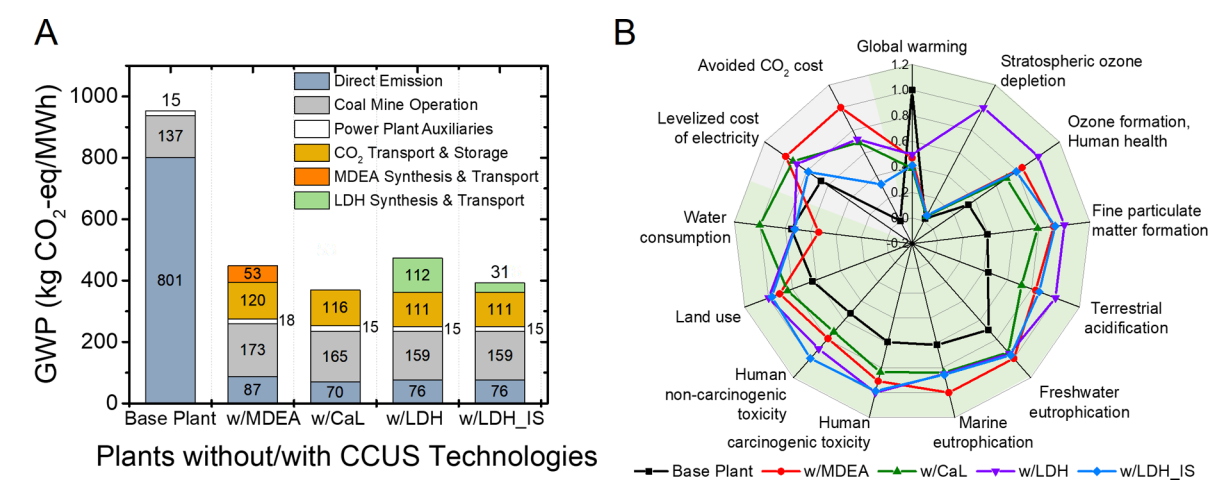


Figure 6. Preliminary life cycle assessment of a typical coal-fired power plant with LDH-based carbon capture. Comparison of decoupled global warming potential (A) and other significant environmental (green background) - economic (gray background) indicators (B) for a typical coal-fired power plant without/with different postcombustion CO₂ capture processes.

previous section (Figure 5B). Figure 6A depicts GWP of the coal power plant without carbon capture and the same plant with different postcombustion approaches. While LDH carbon filters have comparable performance in reducing GHG emissions from coal power plants compared with MDEA and CaL, this emergent technology shows a relatively high GWP mainly due to high emissions from the synthesis and transportation of LDH, which contributes around 24% of total emissions from the plant with LDH. Specifically, we find that the usage of chemical precursors (i.e., Ca(NO₃)₂ and Al(NO₃)₃) emits 89 kg CO₂-eq/MWh, accounting for 79% of total emissions in the synthesis and transportation of LDH. Current nitric acid production often generates nitrous oxide (N_2O) as an undesired byproduct, which is a very potent greenhouse gas with a global warming potential 265 times higher than that of CO2. Hence, it would be highly beneficial to start the LDH synthesis directly from chloride-based precursors since we identified CaAlNO₃-LDH as an inappropriate adsorbent due to its poor thermal stability. Previous studies have demonstrated the synthesis of NiAlCl-LDHs using NiCl₂ and AlCl₃ solutions as electrolytes, proving the feasibility of electrochemical LDH synthesis without using nitrate-based precursors.⁵⁷ LCA analysis shows that GWP of LDH synthesis and transportation could drop from 112 kg of CO₂-eq/MWh to 31 kg of CO₂-eq/MWh if the nitrate-based precursors were to be replaced with chloride-based ones (shown as w/LDH IS in Figure 6A).

The GWP associated with coal mine operations is closely related to the energy expenditures to separate CO_2 since the carbon capture process consumes additional fossil fuels. The amine-based scrubbing process has the highest GWP associated with the coal mine operation, indicating high energy demand involved in such a process. In general, using solid adsorbents for carbon capture reduces the energy cost. Compared with the CaL process, the LDH-based carbon capture process generates slightly lower GWP from the coal mine operation due to the lower thermal energy demands for material rejuvenation and reduced capacity loss over time. It has to be noted that the reported GWP of the CaL process was calculated based on the theoretical enthalpy of calcite decomposition (179 kJ/mol) which might underestimate the energy expenditure in a real system, whereas GWP of the

LDH-based process was calculated using the experimentally determined energy consumption associated with the Joule-heating process.

Besides GWP, Figure 6B compares other important environmental and human health indicators, which have rarely been considered in previous studies of solid adsorbents. In general, all of the current carbon capture technologies would pose an increased environmental impact due to the additional chemicals and energy involved in order to reduce CO₂ emissions from power plants. The LDH-based process is found to have a high stratospheric ozone depletion of 2.14 X 10⁻³ kg CFC-11-eq/MWh, which is mainly due to the usage of nitrate-based chemicals. For the same reason, the LDH-based process has slightly higher ozone formation (0.73 kg of NOxeq/MWh), fine particulate formation (0.62 kg of PM 2.5-eq/ MWh), and terrestrial acidification (1.6 kg of SO₂-eq/MWh) compared with the prevailing MDEA approach. By switching the nitrate-based chemical precursors to chloride-based (shown as w/LDH_IS) chemical precursors, the stratospheric ozone depletion is expected to drop by an order of magnitude, and the other environmental indicators would also become comparable or less than those of the MDEA approach. However, an adverse effect of switching chemical precursors is the increase of human noncarcinogenic toxicity due to the increased usage of hydrochloric acid. Nevertheless, we found that the LDH-based process would not pose an acute threat to the environment and therefore could be a low-temperature and complementary solution to CaL.

Moreover, the economic viability of carbon capture technologies is a critical consideration for their widespread adoption and scalability. One crucial metric in evaluating the competitiveness of power generation methods is the levelized cost of electricity (LCOE). Figure 6B shows that both the CaL and LDH-based processes have similar LCOEs, approximately \$85 per megawatt-hour (MWh). However, the LDH-based process had a slightly higher avoided CO₂ cost (\$45.5 per ton-CO₂) compared to CaL (\$43.7 per ton-CO₂). This difference was attributed to the two-step LDH synthesis approach, which used nitrate-based chemicals as precursors and resulted in a higher GWP. We also identified a potential advantage of the LDH-based process. If a one-step synthesis approach is adopted, using chloride-based chemicals as precursors instead

of nitrate-based ones, the LDH-based process could become more economically viable. By making this change, the GWP is reduced, leading to a lowered avoided CO_2 cost of \$20 per ton- CO_2 and a reduced LCOE of approximately \$75/MWh. This shift could make the LDH-based process more competitive and attractive for large-scale implementation. The MDEA-based process was found to be less economically feasible compared with CaL and LDH -based methods. The higher capital costs, chemical costs, and GWP associated with the MDEA process make it less competitive from both an environmental and economic standpoint.

ASSOCIATED CONTENT

Supporting Information

The Supporting Information is available free of charge at https://pubs.acs.org/doi/10.1021/acs.est.3c03742.

Decoupling the adsorption of water vapor and CO₂; environmental and economic analysis of carbon capture technologies; dominating phases tuned by current density; theoretical calcium and aluminum speciation in the electrolyte; nitrogen adsorption isotherm; FTIR spectrum and TGA data of the carbon fiber substrate; enthalpy of calcite decomposition; change in composition after calcination and rehydration; adsorption kinetics of water vapor and CO₂; activation energy of water vapor and CO₂ adsorption; molar mass of adsorbed water and CO₂; electrothermal rejuvenation of the adsorbent; thermodynamic analysis on the Joule-heating-based material rejuvenation; CO₂ adsorption capacity of solid sorbents (PDF)

LDH inventory, ReCipe-LDHnew, ReCipe-MDEA, ReCipe-CaL, ReCipe-base plant, and TEA (ZIP)

AUTHOR INFORMATION

Corresponding Author

Claire E. White — Department of Civil and Environmental Engineering, Princeton University, Princeton, New Jersey 08544, United States; Andlinger Center for Energy and the Environment, Princeton University, Princeton, New Jersey 08544, United States; orcid.org/0000-0002-4800-7960; Email: whitece@princeton.edu

Authors

Sunxiang Zheng — Department of Civil and Environmental Engineering, Princeton University, Princeton, New Jersey 08544, United States; Andlinger Center for Energy and the Environment, Princeton University, Princeton, New Jersey 08544, United States; orcid.org/0000-0001-8932-3102

Cuihong Song – Department of Civil and Environmental Engineering, Princeton University, Princeton, New Jersey 08544, United States

Maria C. Curria — Department of Civil and Environmental Engineering, Princeton University, Princeton, New Jersey 08544, United States; Andlinger Center for Energy and the Environment, Princeton University, Princeton, New Jersey 08544, United States; orcid.org/0000-0002-3080-8508

Zhiyong Jason Ren — Department of Civil and Environmental Engineering, Princeton University, Princeton, New Jersey 08544, United States; Andlinger Center for Energy and the Environment, Princeton University, Princeton, New Jersey 08544, United States; Occid.org/0000-0001-7606-0331

Complete contact information is available at:

https://pubs.acs.org/10.1021/acs.est.3c03742

Note

The authors declare no competing financial interest.

ACKNOWLEDGMENTS

The authors are thankful for the financial support from the Andlinger Center for Energy and the Environment at Princeton University and the MRSEC seed grant. We acknowledge the use of Princeton's Imaging and Analysis Center, which is partially supported through the Princeton Center for Complex Materials (PCCM), a National Science Foundation (NSF) - Materials Research Science and Engineering Center (MRSEC) program (DMR-1420541 and DMR-2011750). This research used 28-ID-1 of the National Synchrotron Light Source II, a U.S. Department of Energy (DOE) Office of Science User Facility operated for the DOE Office of Science by Brookhaven National Laboratory under Contract No. DE-SC0012704. Special thanks go to Prof. Ange Nizhou and Dr. Nathalie Lyczko who helped with DSC-TGA analysis at IMT Mines Albi.

REFERENCES

- (1) Solomon, S.; Plattner, G.-K.; Knutti, R.; Friedlingstein, P. Irreversible climate change due to carbon dioxide emissions. *Proceedings of the National Academy of Sciences* **2009**, *106* (6), 1704.
- (2) Peters, G. P.; Geden, O. Catalysing a political shift from low to negative carbon. *Nature Climate Change* **2017**, *7* (9), 619–621.
- (3) Chu, S.; Majumdar, A. Opportunities and challenges for a sustainable energy future. *Nature* **2012**, *488* (7411), 294–303.
- (4) Salas, D. A.; Ramirez, A. D.; Rodríguez, C. R.; Petroche, D. M.; Boero, A. J.; Duque-Rivera, J. Environmental impacts, life cycle assessment and potential improvement measures for cement production: a literature review. *Journal of Cleaner Production* **2016**, 113, 114–122.
- (5) Smit, B.; Park, A.-H. A.; Gadikota, G. The grand challenges in carbon capture, utilization, and storage. *Frontiers in Energy Research* **2014**, 2, 55.
- (6) Vitillo, J. G.; et al. Introduction: Carbon capture and separation. *Chemical Reviews* **2017**, *117* (14), 9521–9523.
- (7) Sreenivasulu, B.; Sreedhar, I.; Suresh, P.; Raghavan, K. V. Development trends in porous adsorbents for carbon capture. *Environmental Science & Technology* **2015**, 49 (21), 12641–12661.
- (8) Galan, I.; Glasser, F. P.; Andrade, C. Calcium carbonate decomposition. *Journal of Thermal Analysis and Calorimetry* **2013**, *111* (2), 1197–1202.
- (9) Perejón, A.; Romeo, L. M.; Lara, Y.; Lisbona, P.; Martínez, A.; Valverde, J. M. The calcium-looping technology for CO₂ capture: On the important roles of energy integration and sorbent behavior. *Applied Energy* **2016**, *162*, 787–807.
- (10) He, D.; Ou, Z.; Qin, C.; Deng, T.; Yin, J.; Pu, G. Understanding the catalytic acceleration effect of steam on CaCO₃ decomposition by density function theory. *Chemical Engineering Journal* **2020**, 379, 122348.
- (11) Khan, A. I.; O'Hare, D. Intercalation chemistry of layered double hydroxides: recent developments and applications. *Journal of Materials Chemistry* **2002**, *12* (11), 3191–3198.
- (12) Wang, Q.; Gao, Y.; Luo, J.; Zhong, Z.; Borgna, A.; Guo, Z.; O'Hare, D. Synthesis of nano-sized spherical Mg₃Al-CO₃ layered double hydroxide as a high-temperature CO₂ adsorbent. *RSC Advances* **2013**, 3 (10), 3414–3420.
- (13) Ram Reddy, M. K.; Xu, Z. P.; Diniz da Costa, J. C. Influence of water on high-temperature CO₂ capture using layered double hydroxide derivatives. *Ind. Eng. Chem. Res.* **2008**, 47 (8), 2630–2635. (14) Ram Reddy, M. K.; Xu, Z. P.; Lu, G. Q.; Diniz da Costa, J. C.

Layered double hydroxides for CO₂ capture: structure evolution and regeneration. *Ind. Eng. Chem. Res.* **2006**, 45 (22), 7504–7509.

- (15) Torres-Rodríguez, D. A.; Lima, E.; Valente, J. S.; Pfeiffer, H. $\rm CO_2$ capture at low temperatures (30–80 °C) and in the presence of water vapor over a thermally activated Mg-Al layered double hydroxide. *The Journal of Physical Chemistry A* **2011**, 115 (44), 12243–12250.
- (16) Potter, M. E.; Cho, K. M.; Lee, J. J.; Jones, C. W. Role of alumina basicity in CO₂ uptake in 3-Aminopropylsilyl-grafted alumina adsorbents. *ChemSusChem* **2017**, *10* (10), 2192–2201.
- (17) Watanabe, T.; Liao, J.; Senna, M. Changes in the basicity and species on the surface of Me(OH)₂-SiO₂ (Me = Ca, Mg, Sr) mixtures due to mechanical activation. *J. Solid State Chem.* **1995**, *115* (2), 390–394.
- (18) Otsuka, N. 1.18 Fireside Corrosion. In *Shreir's Corrosion*; Cottis, B., Graham, M., Lindsay, R., Lyon, S., Richardson, T., Scantlebury, D., Stott, H., Eds.; Elsevier: Oxford, 2010; pp 457–481.
- (19) Beruto, D. T.; Botter, R. Liquid-like H_2O adsorption layers to catalyze the $Ca(OH)_2/CO_2$ solid-gas reaction and to form a non-protective solid product layer at $20^{\circ}C$. Journal of the European Ceramic Society **2000**, 20 (4), 497–503.
- (20) Marchi, A. J.; Apesteguia, C. R. Impregnation-induced memory effect of thermally activated layered double hydroxides. *Applied Clay Science* **1998**, *13* (1), 35–48.
- (21) Theiss, F. L.; Ayoko, G. A.; Frost, R. L. Synthesis of layered double hydroxides containing Mg²⁺, Zn²⁺, Ca²⁺ and Al³⁺ layer cations by co-precipitation methods—A review. *Appl. Surf. Sci.* **2016**, 383, 200–213.
- (22) Zhang, X.; Li, S. Mechanochemical approach for synthesis of layered double hydroxides. *Appl. Surf. Sci.* **2013**, *274*, 158–163.
- (23) Ivashkevych, O.; Abeykoon, M.; Adams, J.; Bischof, G.; Dooryhee, E.; Li, J.; Petkus, R.; Trunk, J.; Yin, Z. Hard X-ray pair distribution function (PDF) beamline and END-station control system. *ICALEPCS2019*; 2020.
- (24) Qiu, X.; Thompson, J. W.; Billinge, S. J. PDFgetX2: A GUI-driven program to obtain the pair distribution function from X-ray powder diffraction data. *J. Appl. Crystallogr.* **2004**, *37* (4), *678*–*678*.
- (25) Petrescu, L.; Bonalumi, D.; Valenti, G.; Cormos, A.-M.; Cormos, C.-C. Life Cycle Assessment for supercritical pulverized coal power plants with post-combustion carbon capture and storage. *Journal of Cleaner Production* **2017**, *157*, 10–21.
- (26) Tóth, V.; Sipiczki, M.; Pallagi, A.; Kukovecz, C1.; Kónya, Z.; Sipos, P.; Pálinkó, I. Synthesis and properties of CaAl-layered double hydroxides of hydrocalumite-type. *Chemical Papers* **2014**, *68* (5), 633–637.
- (27) Milagres, J. L.; Bellato, C. R.; Vieira, R. S.; Ferreira, S. O.; Reis, C. Preparation and evaluation of the Ca-Al layered double hydroxide for removal of copper(II), nickel(II), zinc(II), chromium(VI) and phosphate from aqueous solutions. *Journal of Environmental Chemical Engineering* **2017**, *5* (6), 5469–5480.
- (28) Lee, J.-Y.; Gwak, G.-H.; Kim, H.-M.; Kim, T.-i.; Lee, G. J.; Oh, J.-M. Synthesis of hydrotalcite type layered double hydroxide with various Mg/Al ratio and surface charge under controlled reaction condition. *Applied Clay Science* **2016**, *134*, 44–49.
- (29) Fahami, A.; Duraia, E.-S. M.; Beall, G. W.; Fahami, M. Facile synthesis and structural insight of chloride intercalated Ca/Al layered double hydroxide nanopowders. *J. Alloys Compd.* **2017**, 727, 970–977.
- (30) Obata, K.; van de Krol, R.; Schwarze, M.; Schomäcker, R.; Abdi, F. F. In situ observation of pH change during water splitting in neutral pH conditions: impact of natural convection driven by buoyancy effects. *Energy & Environmental Science* **2020**, *13* (12), 5104–5116.
- (31) Rousselot, I.; Taviot-Guého, C.; Leroux, F.; Léone, P.; Palvadeau, P.; Besse, J.-P. Insights on the structural chemistry of hydrocalumite and hydrotalcite-like materials: Investigation of the series $Ca_2M^{3+}(OH)_6Cl\cdot 2H_2O$ (M^{3+} : Al^{3+} , Ga^{3+} , Fe^{3+} , and Sc^{3+}) by X-ray powder diffraction. *J. Solid State Chem.* **2002**, *167* (1), 137–144.
- (32) Bhattacharya, L.; Elzinga, E. J. A comparison of the solubility products of layered Me(II)-Al(III) hydroxides based on sorption

- studies with Ni(II), Zn(II), Co(II), Fe(II), and Mn(II). Soil Systems 2018, 2 (2), 20.
- (33) Wang, W.; Chee, S. W.; Yan, H.; Erofeev, I.; Mirsaidov, U. Growth dynamics of vertical and lateral layered double hydroxide nanosheets during electrodeposition. *Nano Letters* **2021**, *21* (14), 5977–5983.
- (34) Liu, H.-M.; Zhao, X.-J.; Zhu, Y.-Q.; Yan, H. DFT study on MgAl-layered double hydroxides with different interlayer anions: structure, anion exchange, host-guest interaction and basic sites. *Phys. Chem. Chem. Phys.* **2020**, 22 (4), 2521–2529.
- (35) Hibino, T. Anion selectivity of layered double hydroxides: Effects of crystallinity and charge density. *Eur. J. Inorg. Chem.* **2018**, 2018 (6), 722–730.
- (36) Castellote, M.; Fernandez, L.; Andrade, C.; Alonso, C. Chemical changes and phase analysis of OPC pastes carbonated at different CO₂ concentrations. *Materials and Structures* **2009**, 42 (4), 515–525.
- (37) Rodriguez-Blanco, J. D.; Shaw, S.; Benning, L. G. The kinetics and mechanisms of amorphous calcium carbonate (ACC) crystallization to calcite, via vaterite. *Nanoscale* **2011**, 3 (1), 265–271.
- (38) Hou, X.; Kirkpatrick, R. J. Thermal evolution of the Cl–LiAl₂ layered double hydroxide: A multinuclear MAS NMR and XRD perspective. *Inorganic Chemistry* **2001**, *40* (25), 6397–6404.
- (39) Brockner, W.; Ehrhardt, C.; Gjikaj, M. Thermal decomposition of nickel nitrate hexahydrate, Ni(NO₃)₂·6H₂O, in comparison to Co(NO₃)₂·6H₂O and Ca(NO₃)₂·4H₂O. *Thermochim. Acta* **2007**, 456 (1), 64–68.
- (40) Klemkaite, K.; Prosycevas, I.; Taraskevicius, R.; Khinsky, A.; Kareiva, A. Synthesis and characterization of layered double hydroxides with different cations (Mg, Co, Ni, Al), decomposition and reformation of mixed metal oxides to layered structures. *Open Chemistry* **2011**, *9* (2), 275–282.
- (41) Beruto, D.; Searcy, A. W. Use of the Langmuir method for kinetic studies of decomposition reactions: calcite (CaCO₃). *Journal of the Chemical Society, Faraday Transactions 1: Physical Chemistry in Condensed Phases* **1974**, 70 (0), 2145–2153.
- (42) Rives, V. Characterisation of layered double hydroxides and their decomposition products. *Mater. Chem. Phys.* **2002**, *75* (1), 19–25
- (43) Shang, S.; Hanif, A.; Sun, M.; Tian, Y.; Ok, Y. S.; Yu, I. K. M.; Tsang, D. C. W.; Gu, Q.; Shang, J. Novel M (Mg/Ni/Cu)-Al-CO₃ layered double hydroxides synthesized by aqueous miscible organic solvent treatment (AMOST) method for CO₂ capture. *Journal of Hazardous Materials* **2019**, 373, 285–293.
- (44) Zhitova, E. S.; Greenwell, H. C.; Krzhizhanovskaya, M. G.; Apperley, D. C.; Pekov, I. V.; Yakovenchuk, V. N. Thermal evolution of natural layered double hydroxides: Insight from quintinite, hydrotalcite, stichtite, and Iowaite as reference samples for CO₃⁻ and Cl⁻members of the hydrotalcite supergroup. *Minerals* **2020**, *10* (11), 961.
- (45) Xiao, G.; Li, Z.; Saleman, T. L.; May, E. F. Adsorption equilibria and kinetics of CH_4 and N_2 on commercial zeolites and carbons. *Adsorption* **2017**, 23 (1), 131–147.
- (46) Guarín Romero, J. R.; Moreno-Piraján, J. C.; Giraldo Gutierrez, L. Kinetic and equilibrium study of the adsorption of CO_2 in ultramicropores of resorcinol-formaldehyde aerogels obtained in acidic and basic medium. C **2018**, 4 (4), 52.
- (47) Materic, V.; Smedley, S. I. High temperature carbonation of $Ca(OH)_2$. Ind. Eng. Chem. Res. 2011, 50 (10), 5927–5932.
- (48) Rouquerol, J.; Rouquerol, F.; Llewellyn, P.; Maurin, G.; Sing, K. S. Adsorption by powders and porous solids: principles, methodology and applications; Academic Press: 2013.
- (49) Lee, S.-Y.; Park, S.-J. A review on solid adsorbents for carbon dioxide capture. *Journal of Industrial and Engineering Chemistry* **2015**, 23, 1–11.
- (50) Samanta, A.; Zhao, A.; Shimizu, G. K. H.; Sarkar, P.; Gupta, R. Post-combustion CO_2 capture using solid sorbents: A review. *Ind. Eng. Chem. Res.* **2012**, *51* (4), 1438–1463.

- (51) Ma, C.; Urban, J. J. Enhanced CO₂ capture and hydrogen purification by hydroxy metal-organic framework/polyimide mixed matrix membranes. *ChemSusChem* **2019**, *12* (19), 4405–4411.
- (52) Yang, S.; Zhan, L.; Xu, X.; Wang, Y.; Ling, L.; Feng, X. Graphene-based porous silica sheets impregnated with polyethyleneimine for superior CO₂ capture. *Adv. Mater.* **2013**, *25* (15), 2130–2134.
- (53) Ma, W.; Lu, X.; Guan, Y.-F.; Elimelech, M. Joule-heated layered double hydroxide sponge for rapid removal of silica from water. *Environmental Science & Technology* **2021**, 55 (23), 16130–16142.
- (54) Wang, X.; Zhou, S.; Xing, W.; Yu, B.; Feng, X.; Song, L.; Hu, Y. Self-assembly of Ni-Fe layered double hydroxide/graphene hybrids for reducing fire hazard in epoxy composites. *Journal of Materials Chemistry A* **2013**, *1* (13), 4383–4390.
- (55) Pradhan, B.; Srivastava, S. K. Layered double hydroxide/multiwalled carbon nanotube hybrids as reinforcing filler in silicone rubber. *Composites Part A: Applied Science and Manufacturing* **2014**, 56, 290–299.
- (56) Zhao, M.; He, X.; Ji, G.; Song, Y.; Zhao, X. Zirconia incorporated calcium looping absorbents with superior sintering resistance for carbon dioxide capture from in situ or ex situ processes. *Sustainable Energy & Fuels* **2018**, *2* (12), 2733–2741.
- (57) Zhang, J.-j.; Zhang, T.-a.; Feng, S. Ni-Al layered double hydroxides electrodeposition from a chloride solution. *Arabian Journal of Chemistry* **2021**, *14* (7), 103208.